Impact of Spatial Hole Burning and Linewidth Enhancement Factor on Distributed-Feedback Quantum Cascade Lasers: A Comprehensive Design Analysis

Sara Zaminga, Lorenzo Columbo, Carlo Silvestri, Mariangela Gioannini, *Member, IEEE*, and Frédéric Grillot

***Abstract*—In this article, we use a time-domain traveling-wave approach with a coupled-mode theory to describe the dynamics of a mid-Infrared (MIR) Quantum Cascade Laser (QCL) in the Distributed-Feedback (DFB) configuration. We demonstrate that linewidth enhancement factor (LEF) and spatial hole burning (SHB) play a crucial role in influencing the device's single-mode behavior. Neglecting them leads to an overestimation of the interval of pump currents granting single-mode emission and to an inaccurate simulation of the QCLs' multimode dynamics. By taking into account these two mechanisms, we inspect the combined action of the DFB grating's coupling strength and end facets' reflectivity. The purpose is to supply designers with a guideline to achieve the optimal structure for efficient single-mode emission, which is a highly required specification in manifold applications, like free-space optical communication. Numerical simulations are in good agreement with experimental findings relative to a DFB QCL operating at 9.34 μm.**

***Index Terms*—Coupled-mode theory, distributed-feedback, effective semiconductor maxwell-bloch equations, linewidth enhancement factor, quantum cascade laser, spatial hole burning.**

I. Introduction

NOWADAYS, the mid-infrared (MIR) spectral region is of particular interest to research and industry because of its versatile properties, depending on the application. Medical diagnostics, pollution monitoring, environment sensing are currently available technologies based on precision spectroscopy [1], identifying gas- and liquid-phase chemicals, since they display characteristic absorption lines in this region. Free-space optics (FSO) [2] is progressively perceived as a valid solution to overcome the several radio-frequency (RF) and optical fiber bottlenecks. Specifically, the MIR domain features low atmospheric absorption [3], [4], low resistance to turbulence [5] and low scattering (both Mie, Geometric) [6]. Moreover, it tends to have better penetration through both good and inclement weather conditions, like haze and fog [7]. Finally, the thermal black-body radiation shows a strong background in the 8-14 μm range, providing the means for highly-secure and high-bandwidth communications for defense applications [8], [9].

The Quantum Cascade Laser (QCL) is an outright semiconductor technology, based on unipolar intersubband transitions for light generation [10]. Thanks to its engineered superlattice heterostructure, this stable and compact source is widely tunable across the infrared spectrum, being compliant with the aforementioned applications. Though, most of the latters demand devices operating at a single desired frequency. Optical communication systems require dynamic single-mode lasers with a narrow linewidth as transmitters to increase the data transmission rates. Various techniques exist for achieving single-mode emission in QCLs, prominently including slotted waveguides [11] and distributed feedback (DFB) [12]. The former manipulates the waveguide structure with strategically placed slots or gaps to control mode profiles. However, while effective, the design intricacies and fabrication complexities associated with achieving precise single-mode emission in slotted waveguides can pose challenges. In contrast, DFB lasers offer an established and robust approach to achieving single-mode emission [13]. By integrating a periodic grating structure within the laser cavity, DFB lasers provide stable single-mode operation with a narrow linewidth. Their proven performance in providing stable, high-quality single-mode output, along with their well-established fabrication processes, positions DFB lasers as a superior choice for applications requiring precise and reliable single-mode emission in various fields, including telecommunications, sensing, and scientific instrumentation. Yet, fabricating a DFB grating involves costly high-resolution technological techniques, to ensure robustness and coupling strength. Many designs (e.g., buried gratings, top gratings, etc.) have been proposed along the years for reducing the losses, and achieving CW operation, circumventing thermal issues [14],

Manuscript received 18 January 2024; revised 22 February 2024; accepted 1 March 2024. Date of publication 6 March 2024; date of current version 8 April 2024. This work was supported in part by the Direction Générale de l'Armement (DGA), and in part by the Air Force Office Of Scientific Research (AFSOR) under Grant FA8655-22-1-7032. *(Corresponding author: Sara Zaminga.)*

Sara Zaminga is with the LTCI Télécom Paris, Institut Polytechnique de Paris, 91120 Palaiseau, France (e-mail: sara.zaminga@telecom-paris.fr).

Lorenzo Columbo and Mariangela Gioannini are with the Dipartimento di Elettronica e Telecomunicazioni, Politecnico di Torino, 10129 Torino, Italy.

Carlo Silvestri is with the School of Electrical Engineering, Computer Science, The University of Queensland, Brisbane, QLD 4072, Australia.

Frédéric Grillot is with the LTCI Télécom Paris, Institut Polytechnique de Paris, 91120 Palaiseau, France, and also with the Center for High Technology Materials, University of New-Mexico, Albuquerque, NM 87106 USA.

Digital Object Identifier 10.1109/JPHOT.2024.3373805

© 2024 The Authors. This work is licensed under a Creative Commons Attribution 4.0 License. For more information, see https://creativecommons.org/licenses/by/4.0/

[15]. Yet, manifold aspects regarding the dynamics of these lasers are to be inspected on a theoretical viewpoint. Indeed, many physical mechanisms can drive a laser from single-mode to a multimode regime, like spatial hole burning (SHB), non-zero linewidth enhancement factor (LEF) [16], saturable absorption and self-phase modulation [17], [18], [19]. QCLs dynamics is different than conventional diode lasers', because of the picosecond-scale gain recovery process [20]. This turns out in a population grating induced by the standing-wave pattern originated by the counterpropagating forward E^+ and backward E^- electric fields in Fabry-Perot (FP) QCLs. The period Λ of this carriers grating is around $\lambda_0/2$ (where λ_0 is the emission wavelength in the semiconductor waveguide), resulting longer than the typical diffusion length in FP QCLs. This is in contrast with standard diode lasers, where diffusion occurs on a timescale comparable to the recombination time. Therefore, whereas the nonuniform distribution of the population inversion is washed out by diffusion in conventional diode lasers, it is present and responsible for multimode operation in FP QCLs [21]. Yet, in FP QCLs, spatial hole burning might also be originated by the nonuniform variation of the field slowly varying envelope along the laser, whose period is comparable to the cavity size (hundreds of μm) and, thus, some orders of magnitude longer than the period of the carriers grating Λ. Therefore, we denote as 'fast' SHB the population grating induced by the standing-wave pattern in the laser cavity. We define as 'slow' SHB the carrier spatial modulation induced by the nonuniform variation of the field slowly varying envelope. The slow SHB causes slow photon and carrier distributions inside the cavity, and variation of refractive index. The slow SHB is affected by the DFB design, including the coupling strength and the facets' coating. Since the optical gain and the refractive index are dependent on the carrier density, this will, especially in DFB lasers, change the optical properties of the laser cavity. As an instance, it causes a longitudinal variation of the Bragg wavelength, affecting the selectivity of the cavity of the laser, due to a deterioration of side-mode suppression. Moreover, the presence of this slow SHB in DFB lasers also influences the FM-response and may result in a less flat FM-response [22]. It also results in intermodulation distortion, chirp [23] and mode hopping. In addition, although the initial prediction of a zero LEF due to the unipolar character of the laser transition [10], more recent theoretical [24] and experimental works [25], [26], [27] demonstrate a smaller but non-zero LEF in MIR QCLs, compared to conventional bipolar lasers. Higher values of LEF are associated to a higher phase-amplitude coupling of the electric field, favoring the occurrence of multi-mode regimes [16]. Hence, the purpose of this work is to consider the DFB configuration to extend the formalism of Effective Semiconductor Maxwell-Bloch Equations (ESMBEs) proposed in [28] and [16] for the FP and the innovative ring geometries respectively. This has been done in the framework of the coupled-mode theory [29]. By employing this rigorous approach, we achieve a comprehensive investigation of the mechanism responsible for single-mode selection in DFB QCLs. The goal of this paper is to highlight the important effect of non-zero LEF and fast SHB on QCLs multimode dynamics and single-mode emission, by considering their interplay with the DFB design. Remarkably, to the best of our knowledge, this work represents the first investigation of this kind, signifying an important advancement in the field.

II. Numerical Model: Equations and Parameters of Simulation

Single-mode selection refers to the capability of selecting a precise laser's emission mode using a DFB grating. The DFB grating introduces a periodic variation in refractive index, which results in the formation of a photonic gap, also known as a stopband, centered around the Bragg frequency. The DFB configuration enables the laser to emit longitudinal modes situated on both sides of this photonic gap. Among these modes, the two modes located at the extremes of the photonic gap exhibit the lowest lasing thresholds when compared to all other possible longitudinal modes supported by the DFB. The grating structure enforces wavelength-specific feedback for the laser emission, resulting in coupling between forward and backward-traveling waves. This interaction is quantified by the grating's coupling strength. It is a complex number $\kappa = j\kappa_{\mathrm{DFB}}e^{j\Phi}$, according to the theory in [29]. In order to take this phenomenon into account, a consequent modification of the numerical model is required. To numerically solve the resulting Time-Domain (TD) Traveling-Wave (TW) model, the split-step method proposed in [37] is applied. With respect to the model detailed in [28], E^+, E^- satisfy the approximated coupled (1):

$$\frac{\partial}{\partial z}\begin{bmatrix} E^+(z,t) \\ E^-(z,t) \end{bmatrix} = \begin{bmatrix} 0 & -i\kappa \\ i\kappa^* & 0 \end{bmatrix}\begin{bmatrix} E^+(z,t) \\ E^-(z,t) \end{bmatrix} \tag{1}$$

Table I reports the values of the parameters used in simulations. To determine the latter, a real device emitting in the third atmospheric window in the DFB configuration is taken as a reference. Its DFB design is based on metal top-index grating, as extensively described in [14] and [15]. The device emits at 9.34 μm, with threshold current around 298 mA. Its single-mode operation is granted on a range of drive currents up to around 380 mA, above which multimode operation is observed. The carrier lifetime, as well as the polarization decay rate are chosen according to [33]. The reflectivity of the end facets are set to match the design of the QCL under study. The back facet is coated with a high-reflectivity layer (HR, 99%), the front facet is left cleaved (32%). Depending on the applications, devices are fabricated to have a low or a high κ_{DFB}. We assume $\kappa_{\mathrm{DFB}} \leq 10$ cm^{-1} from our device's specifications. The higher κ_{DFB}, the more efficient the FP modes rejection. Though, if it is too large, the threshold gain difference between stopband edge modes is reduced and the laser becomes multimode. It has been experimentally [38] and theoretically [39] demonstrated that lasers with high κ_{DFB} are characterized by a deteriorated side-mode suppression, even for low or moderate pump currents, because of slow SHB. To roughly retrieve the experimental value of κ_{DFB} from the device under study, we refer to the method described in [40]. It consists in determining the width of the stopband below threshold, being it proportional to κ_{DFB} L, a dimensionless quantity including the length of the grating L (see Fig. 1(b)). Being L = 2 mm and the measured stopband equal to

TABLE I
MATERIAL AND DEVICE PARAMETERS USED IN SIMULATIONS FOR THE QCL IN THE DFB CONFIGURATION

Physical Parameters		Geometrical Parameters		Simulation Duration and Time Step	
τ_e (ps) [30]–[32]	1	R_{front} [2]	32 %	T_{sim} (ns)	500
τ_d (fs) [31]–[33]	320	R_{back} [2]	99 %	ΔT (fs)	30
Γ_c	0.127	L (mm) [2]	2		
f_0 (μm^3) [30]	1.1×10^{-7}	V (μm^3) [30]	2240		
LEF [34] [1]	1.2	κ_{DFB} (cm^{-1}) [1]	9		
η_i [35]	85 %				
α_{tot} (cm^{-1}) [36]	8.9				
λ_0 (μm) [2]	9.34				

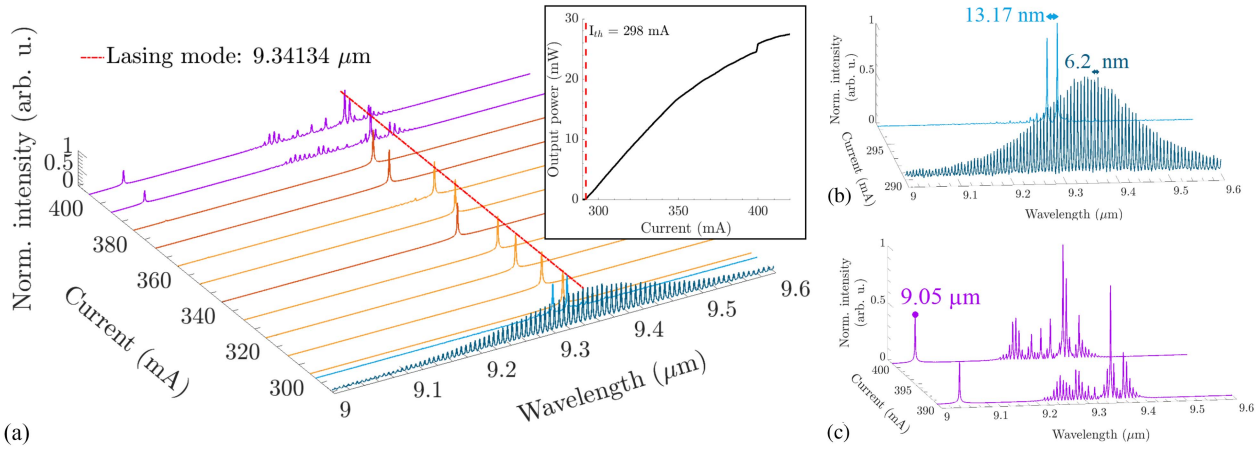

Fig. 1. (a) Map of optical spectra of the DFB QCL under study, obtained with FTIR. The bias current is swept from 290 mA to 400 mA in steps of 10 mA. (b) At 290 mA the laser is well below threshold. The FP laser mode separation is around 6.2 nm, corresponding to nearly 22 GHz. When the current is set slightly below threshold, at 297.5 mA, a stopband of 13.17 nm is observable. The FP side modes are suppressed. Only the two competing side modes (low frequency mode, nearly 9.32 μm, high frequency mode, nearly 9.34 μm) at the edges of the stopband are evident. At 298 mA, the laser turns on. Up to 380 mA, the laser is single-mode, emitting at 9.34 μm. Mode hopping at 9.32 μm is observed at 340 mA and 370 mA. (c) Above 470 mA, the laser becomes multi-mode, showing also a transverse mode at 9.05 μm. (inset) Light-Intensity (LI) curve of the DFB QCL under study.

13.17 nm, we retrieve a $\kappa_{DFB} = 9$ cm^{-1}, confirming the device's specifications.

With respect to the model in [16], [28], the total losses are increased, accounting for the presence of the DFB grating. This quantity is set according to the experimental findings in [36], relative to a DFB QCL. Finally, the LEF is chosen to match the dynamics of the tested DFB QCL. Simulations with LEF = 1.2 are in good agreement with the experiments[1] [2].

III. NUMERICAL RESULTS

A. Simulation of a DFB QCL Emitting At 9.34 μm

In this section, we compare the experimental results in Fig. 1 with those in Fig. 2. Both represent a map of optical spectra when the bias current is swept. Fig. 1(a) is experimentally obtained at 293 K with a pump sweep from 290 mA to 400 mA. The current limitation to 400 mA is for safety reason. The optical spectra are provided by Fourier Transform Infrared Spectroscopy (FTIR). Fig. 2(a) represents the map obtained from simulations of a device emulating the behavior of the one under study (see Table I). In both cases, the laser turns on around 295 mA, emitting single-mode up to 380 mA. Fig. 2(b) highlights a numerical stopband of nearly 11.38 nm, which is very close to the measured stopband of 13.17 nm in Fig. 1(b). When the laser is single-mode, the side-mode-suppression-ratio (SMSR) retrieved from simulations is >70 dB (see Fig. 2(c)): the single-mode selection is thus effective. Though, in the experimental map a red shift of the lasing mode is detectable, due to a wavelength's thermal dependence, not included in the model and estimated to be roughly 137.43 pm/mA.

When the laser switches to multimode operation, simulations reveal two multimode dynamics. From 380 mA to 410 mA (see Fig. 2(d)), harmonic states with an average separation of nearly 154 GHz are depicted, independently from the pumping. 154 GHz is approximately 7 × FSR, that is 7 × the free-spectral-range (or mode spacing) above threshold. Similarly, the measurements from the device under analysis show envelopes of the spectra consisting of multiple peaks, with an average separation of 110 GHz, independently of the pumping. The nature of such harmonic states can be related to the fact that at a significantly high pumping level, named instability

[1]Parameters extracted from measurements
[2]Parameters from vendor's specifications

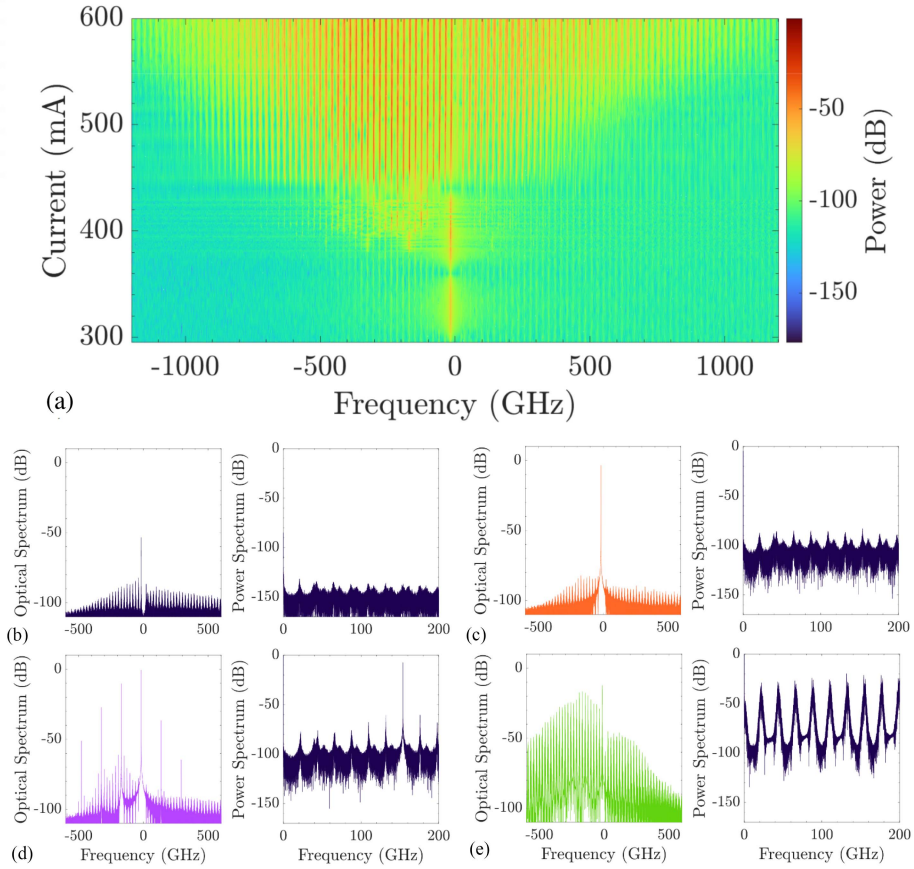

Fig. 2. (a) Optical spectra maps for the DFB configuration, with the parameters of simulations in Table I. The quantity $f - f_0$ ($f_0 = \frac{c}{\lambda_0}$) is represented along x. Along y, the bias current is swept from 300 mA to 600 mA. (b-e) Zoom of optical and RF spectra for a bias current of: (b) 294 mA. The laser is off. (c) 330 mA. The laser is single-mode, with SMSR>70 dB. (d) 380 mA. The laser is multi-mode, with harmonic states equally spaced of nearly 154 GHz = 7FSR. The SMSR < 20 dB. The fundamental beat note in the RF spectrum is 154 GHz. (e) 470 mA. The laser is multimode, with dense states equally spaced of nearly 22 GHz = FSR. The SMSR < 20 dB. The fundamental beat note in the RF spectrum is 22 GHz. Its harmonics are at multiples of 22 GHz.

threshold, longitudinal cavity modes, that are resonant with the Rabi frequency, get enough parametric gain to move above threshold [41]. This might be possible since the Rabi frequency is proportional to the square root of the pump distance from threshold and inversely proportional to the square root of the carriers decay rate [42], which is of the order of 1 ps in QCLs. Consequently, the Rabi frequency in a QCL is of hundreds of GHz or few THz [41], [43], and thus comparable with a multiple of the cavity FSR. Our simulations and experiments are in good agreement with these literature findings. Future studies will concentrate on the estimation of the Rabi frequency from our model, in order to rigorously confirm this picture and provide a possible interpretation of the origin of the observed harmonic states.

When the drive current is further increased in simulations ($>$ 410 mA, see Fig. 2(e)), 22-GHz-spaced dense states are observed. The overall behavior is strongly consistent with observations in [41], [44]. Above 380 mA, the experimental optical spectra exhibit a high order transverse mode around 9.05 μm (separation of nearly 288 GHz from the main longitudinal mode), that is not detectable from Fig. 2(a), since the contribution of high order transverse modes is not taken into account in the current model. The real device also displays the phenomenon of mode hopping between two competing lasing modes at nearly 9.34 μm and 9.32 μm. Their distance does not coincide with either the stopband or the FSR. It is indeed approximately 26.5 nm, which means 4 $\times$ FSR and 2 $\times$ the stopband. The end-facet mirrors might play a role in this phenomenon, since they give reflections that constructively and destructively interfere with DFB modes in the laser cavity. This interference affects the mirror loss of each mode, and can determine which mode lases. It is true that facets reflectivities are included in the model; though, they are real quantities. So, additional complications arising from an indeterminate phase with respect to the grating in the real device are not considered. A detailed analysis on the impact of end-facet mirrors is found in [36], [45].

Finally, model validation derives from setting $\kappa_{\mathrm{DFB}} = 0$ cm^{-1} (thus simulating a FP laser), leaving unchanged all the other parameters from Table I. The expected results from simulations in Fig. 3 depict the typical map of a QCL in FP configuration: the emission is purely multimode, with 22-GHz spacing. The threshold current is approximately 355 mA, 20% higher than 295 mA observed with $\kappa_{\mathrm{DFB}} = 9$ cm^{-1}. This conclusion meets the expectations, since the increased threshold is due to the decreased κ_{DFB}.

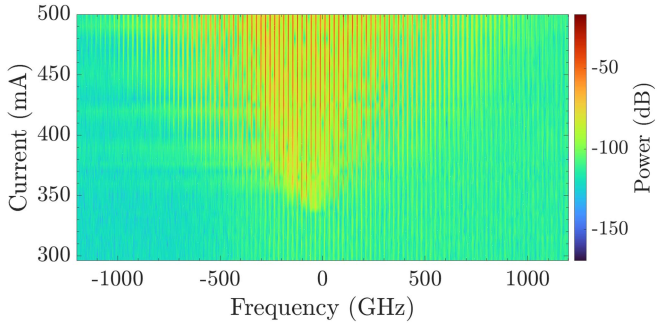

Fig. 3. Optical spectra maps for FP configuration ($\kappa_{\text{DFB}} = 0\ \text{cm}^{-1}$.). The quantity $f - f_0$ ($f_0 = \frac{c}{\lambda_0}$) is represented along x. Along y, the bias current is swept from 300 mA to 500 mA.

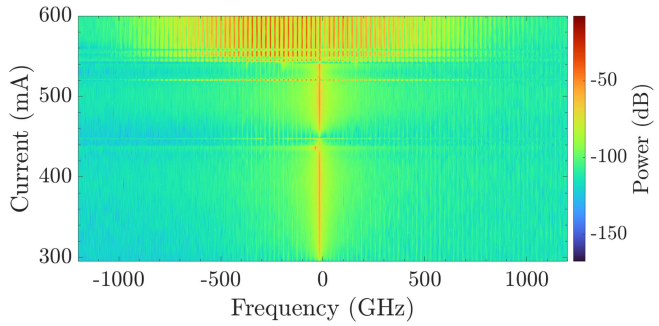

Fig. 4. Optical spectra maps for DFB configuration, with the parameters of simulations in Table I. The fast SHB is numerically zeroed. The quantity $f - f_0$ ($f_0 = \frac{c}{\lambda_0}$) is represented along x. Along y, the bias current is swept from 300 mA to 600 mA.

B. Impact of Fast SHB and LEF on QCL Dynamics

In FP QCLs, the primary mode induces a population grating. This is an incoherent instability and corresponds to the fast contribution of SHB, and consists in a spatial modulation of the inversion, and a consequent modulation of the gain. As the laser pumping is increased, the carriers and gain modulations become stronger, so the primary mode experiences a gain saturation heavier than any other higher order mode. Thus, the single mode regime becomes unfavorable, and additional modes are excited. Since the fast SHB is negligible in conventional lasers (being whashed out by diffusion, as discussed in the Introduction section), the studies in literature only focus on alleviating slow SHB in laser diodes dynamics, developing pertinent numerical methods and special laser structures [46]. From a numerical point of view, slow SHB is intrinsically included in the TDTW model that accounts for slow spatial distribution of the optical field and carriers. A negligible fast SHB is never a typical condition for a QCL. Nevertheless, in our model, it can be forced to zero, in order to study its impact on the QCLs dynamics. Fig. 4 shows that single-mode emission is observed for a current range 130% higher with respect to Fig. 2, because the absence of fast SHB increases the current at which multimode emission turns on. In other words, single-mode emission is strongly overestimated if fast SHB is not taken into account. We suppose that it is the presence of fast SHB as the latter triggers single-mode instability, and thus multimode operation, as previously explained. On the contrary, Fig. 4 depicts dense states only in a multimode regime. Fast SHB is not only responsible for the lowering of the instability threshold and worsening of single-mode emission, but also for shaping the envelope of the QCL's optical spectrum. Besides, LEF promotes a coupling between amplitude and phase of the electric field. The higher the LEF, the higher this coupling, so the easier the occurrence of multimode emission. By comparing Figs. 2(a) and 6 where LEF = 2, the shift to multimode operation is observed around 345 mA, meaning a reduction of single-mode selection efficiency of around 65 %. Also in this case, multimode operation discloses in harmonic states followed by dense states when the drive current increases. Hence, contrarily to what happens when zeroing fast SHB, the shape of the optical spectra map is preserved. It is worth mentioning that LEF is constant throughout the simulations when sweeping the pump current. Experimental studies, though, demonstrate a slightly increasing LEF with the raising of the pump [25]. Finally, if one follows the theory and set LEF = 0, the bias range granting single-mode emission is approximately 4× that of Fig. 2(a). This effect is further enhanced when fast SHB and LEF are simultaneously zeroed, as in Fig. 5(b), that shows single-mode behavior also for a pump of 800 mA. It is worth noticing that the phenomenon of mode hopping is particularly evident when fast SHB is included.

C. Guidelines for the DFB Design

The performance of a device, e.g. single-mode selection and power output, are profoundly affected by the coupling strength and the presence of mirrors. The focus of this section is thus to provide the optimal design in terms of extension of the range of pump currents granting single-mode emission. Three combinations of end facet mirrors are simulated in this work, reproducing the most employed solutions in the marketplace:

- $R_{\text{front}} = 32\%$, $R_{\text{back}} = 99\%$. The front facet is left cleaved. A high-reflective coating is deposited on the back facet. The latter is particularly useful for minimizing losses due to light escaping from the back facet. By increasing the reflectivity, more of the laser light is kept within the laser cavity, which can lead to higher output power and better overall laser efficiency. This configuration corresponds to that of the laser under study.
- $R_{\text{front}} = 5\%$, $R_{\text{back}} = 99\%$. A low-reflective coating is deposited on the front facet. An AR coating helps to reduce the feedback that can destabilize the laser operation (e.g. mode hopping), and to decrease the total losses of the DFB modes.
- $R_{\text{front}} = 32\%$, $R_{\text{back}} = 32\%$. Both the facets are left cleaved.

The reflectivity of the mirrors is assumed to be a real number, since the presence of a phase component is neglected. In reality, light-material interference effects, intrinsic properties of coating materials and fabrication variations make this parameter complex [36], [45]. To emphasize the impact of the interplay of the coupling strength with mirrors deposition on the end facets,

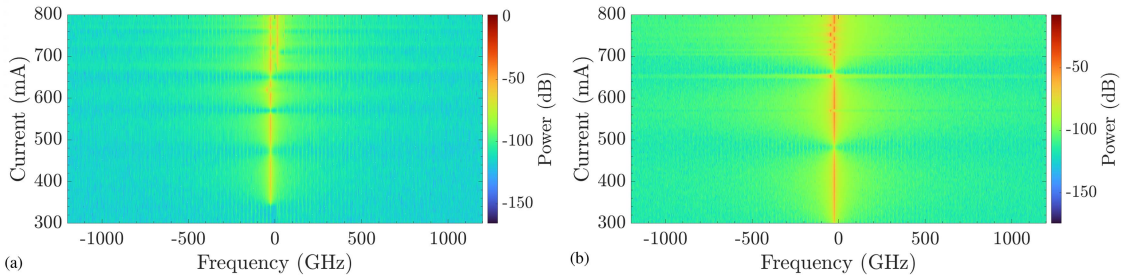

Fig. 5. Optical spectra maps for the DFB configuration, with LEF = 0, setting the remaining parameters of simulations as in Table I. The quantity $f - f_0$ ($f_0 = \frac{c}{\lambda_0}$) is represented along x. Along y, the bias current is swept from 300 mA to 800 mA. (a) The fast SHB is included in the model. (b) The fast SHB is numerically zeroed.

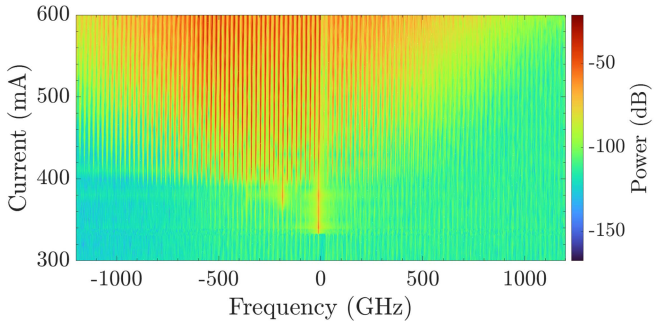

Fig. 6. Optical spectra maps for DFB configuration, with LEF = 2. The quantity $f - f_0$ ($f_0 = \frac{c}{\lambda_0}$) is represented along x. Along y, the bias current is swept from 300 mA to 600 mA.

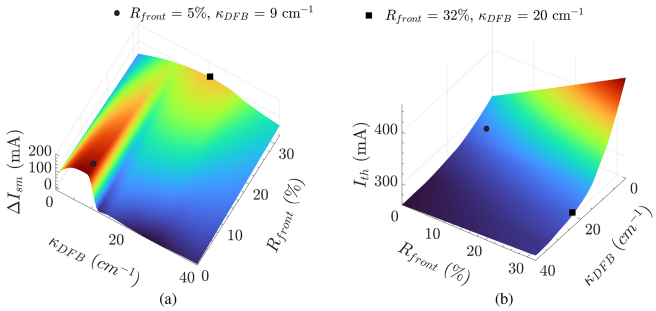

Fig. 7. 3D map for (a) ΔI_{sm} and (b) I_{th} as a function of κ_{DFB} and R_{front}. In (a), (b), the black circle corresponds to (κ_{DFB}, R_{front}) = (9 cm^{-1}, 5%), being the optimal design choice for single-mode emission enhancement. The black square corresponds to (κ_{DFB}, R_{front}) = (20 cm^{-1}, 32%), being the optimal choice when AR coating is not deposited on the front facet of the device.

Fig. 7(a) depicts the area of single-mode emission when varying κ_{DFB} from 0 cm^{-1} to 40 cm^{-1}, and R_{front} from 0% to 32%, with fixed R_{back} = 99%. Single-mode efficiency is expressed in terms of Δ I_{sm}, which is the width of the interval of pump currents where we observe single-mode emission (SMSR > 20 dB). (κ_{DFB}, R_{front}) = (9 cm^{-1}, 5%) displays the optimal value to enhance single-mode area for a device with physical parameters in Table I (black circle in Fig. 7, approximately 2×Δ I_{sm} of the tested QCL). In general, when R_{front} = 5% (AR coating is employed), wider ΔI_{sm} can be measured, for smaller κ_{DFB}, with respect to leaving R_{front} = 32% (cleaved). Yet, the optimization of Δ I_{sm} occurs for a narrow range of κ_{DFB} (roughly, from 5 cm^{-1} to 10 cm^{-1}). Diversely, the efficiency of single-mode selection rapidly drops, and the laser exhibits single-mode behavior for a very limited range of pump currents. On the contrary, a cleaved front facet reduces the maximum Δ I_{sm}, but a larger κ_{DFB} interval grants for an acceptable ΔI_{sm}. Summarily, the augmented asymmetric mirror configuration can enhance single-mode operation by favoring the lasing of a particular longitudinal mode. However, when combined to the action of the DFB grating, the κ_{DFB} necessary for the optimization of single-mode emission is smaller. From a fabrication viewpoint, unavoidable variations in technological processes regarding the DFB grating structure can be highly detrimental if AR coating is employed. Fig. 7(b) exhibits the variation trend for the threshold current I_{th}: the higher R_{front} and κ_{DFB}, the larger I_{th}. In fact, the deposition of AR coating on the front facet reduces the amount of optical feedback into the laser cavity and decreases the threshold current of the laser. Fig. 8 depicts the optical and RF spectra when the pump is fixed at 380 mA, R_{front} = 32%, R_{back} = 99%, but κ_{DFB} is swept from 0 cm^{-1} to 40 cm^{-1}, in steps of 10 cm^{-1}. When κ_{DFB} = 0 cm^{-1}, the laser is in its FP configuration. When κ_{DFB} = 10 cm^{-1}, κ_{DFB} is not optimized, so 157-GHz-spaced harmonic states arise. The optimal κ_{DFB} value is around 20 cm^{-1}, where the laser is still single-mode at 380 mA, with a SMSR > 50 dB. Though, single-mode selection worsens with κ_{DFB} > 20 cm^{-1}: a high κ_{DFB} is desired for FP-modes rejection but if it is too large, the discrimination between stopband edge modes is reduced and the laser becomes bimodal (see Fig. 8(d) and (e)). Therefore, when κ_{DFB} > 20 cm^{-1}, the origin of multimode emission is not the reach of the instability threshold due to SHB and non-zero LEF, but the inability of the DFB grating in stopband edge modes discrimination. Fig. 9 delineates the multimode regimes from the simulations of three DFB QCLs, whose parameters are those in Table I, differing only for their end facets' reflectivity (respectively R_{front} = 32%, R_{back} = 99%, R_{front}5%, R_{back} = 99%, R_{front} = 32%, R_{back} = 32%). For each device, simulations respectively including and zeroing fast SHB have been carried out. In terms of QCL dynamics, we identify a common trend when fast SHB is included: the laser turns on, revealing single-mode behavior. When it switches to multimode operation, harmonic states and consecutively dense states are observed. The exception is the laser with AR coating, displaying harmonic states only. Shifts from harmonic to dense states and viceversa

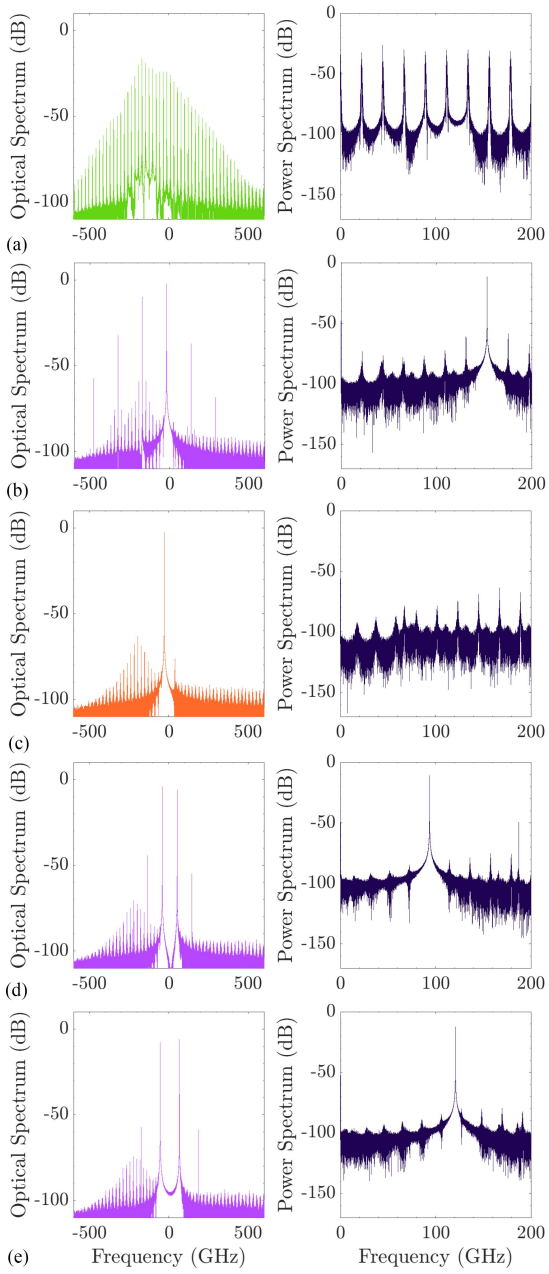

Fig. 8. Optical and RF spectra for the parameters of simulation in Table I, varying κ_{DFB}. (a) 0 cm^{-1}. The laser in the FP configuration is just above threshold, and in multi-mode operation (22-GHz-spaced dense states, SMSR $<$ 5 dB. The fundamental beat note in the RF spectrum is 22 GHz). (b) 10 cm^{-1}. The laser is multi-mode (157-GHz-spaced harmonic states, SMSR $<$ 5 dB. The fundamental beat note in the RF spectrum is 157 GHz). (c) 20 cm^{-1}. The laser is single-mode (SMSR$>$60 dB). (d) 30 cm^{-1}. The laser is multi-mode (90-GHz-spaced harmonic states, SMSR $<$ 5 dB. The fundamental beat note in the RF spectrum is 90 GHz). (e) 40 cm^{-1}. The laser is multi-mode (124-GHz-spaced harmonic states, SMSR $<$ 5 dB. The fundamental beat note in the RF spectrum is 124 GHz).

are noted for the device with cleaved facets. This behavior has been also experimentally confirmed in [44]. Table II reports the devices' figures of merit (FoMs) describing their performance, comparing the results with and without fast SHB effect. η_d is the differential efficiency and it is the efficiency by which the input pump is converted into signal power. With respect to a real

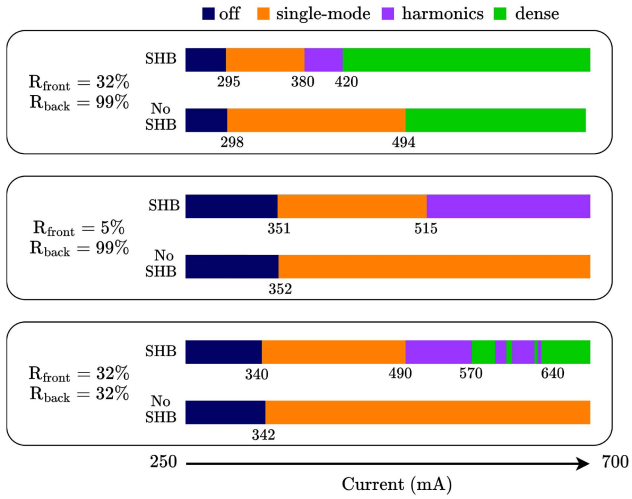

Fig. 9. Dynamics' regimes for QCLs with different end facets' coating: R_{front} = 32%, R_{back} = 99%; R_{front} = 5%, R_{back} = 99%; R_{front} = 32%, R_{back} = 32%. Simulations' results including and excluding fast SHB are reported. Four main regimes are identified: Navy blue (off), orange (single-mode), purple (harmonic states), green (dense states). When zeroing fast SHB, simulations are totally erred in single-mode efficiency and multimode behavior. Harmonic states disappear; dense states are observed only for the case.

TABLE II
COMPARISON OF THE PERFORMANCE OF THREE DFB QCLS WITH DIFFERENT END-FACETS REFLECTIVITY

End-facet reflectivities	**Figure of Merit (FoM)**		
		SHB	no SHB
R_{front}=32%, R_{back}=99%	I_{th}	295 mA	298 mA
	ΔI_{sm}	85 mA	196 mA (+130%)
	η_d	45%	88%
R_{front}=5%, R_{back}=99%	I_{th}	351 mA	352 mA
	ΔI_{sm}	164 mA	$>$ 348 mA ($>$ +112%)
	η_d	98 %	137%
R_{front}=32%, R_{back}=32%	I_{th}	340 mA	342 mA
	ΔI_{sm}	150 mA	$>$ 358 mA ($>$ +138%)
	η_d	41%	62%

device, η_d is overestimated because of an underestimation of the losses of the laser in simulations (i.e. temperature effects are not included in the model). In fact, η_d of the QCL under study is 29% (see inset of Fig. 1), whereas its value from simulations is 45%. The deposition of an AR coating on the front facet allows η_d to be more than doubled with respect to leaving as cleaved the front facet. The improvement, though, does not only regards the power efficiency, but also the single-mode selection. With an AR coating on the front, Δ I_{sm} increases of a factor 2. A similar improvement is observed when both facets are cleaved, even if η_d is critically worsened. We can conclude by stating that asymmetric mirror configurations improve the ability to choose a specific longitudinal mode for single-mode emission [13].

When fast SHB is numerically zeroed, ΔI_{sm} is heavily overrated, as displayed in Table II. The same holds for η_d, getting an unrealistic estimation beyond 100% when $R_{front} = 5\%$. The QCL dynamics is single-mode up to 700 mA, for $R_{front} = 5\%$, $R_{back} = 99\%$ and $R_{front} = 32\%$, $R_{back} = 32\%$. For what concerns the device simulating the conditions of operation of the tested QCL, it only shows 22-GHz dense states after the switching to multimode operation. Harmonic states disappear, signifying the massive role of fast SHB in decreasing the instability threshold and determining the shape of the optical spectrum.

IV. Conclusion

We adopted a new TDTW model based on a set of ESMBEs and a coupled mode approach to simulate the dynamics of DFB QCLs. We managed to qualitatively reproduce experimental findings relative to a DFB QCL operating at 9.34 μm in continuous-wave and room-temperature conditions. We underline the substantial impact of fast SHB and non-zero LEF on the QCL dynamics. It is indisputable how powerful is fast SHB in shaping the multimode behavior of QCLs, rending their dynamics extremely diverse with respect to conventional lasers. Neglecting fast SHB during the design of a DFB QCL induces a thoroughly inaccurate assessment of the interval of drive currents permitting single-mode emission. According to the application, stringent requirements must be fulfilled, but this becomes less feasible by exploiting an unreliable modeling. A large overestimation of single-mode efficiency also derives from zero LEF. In light of this analysis, only geometrical parameters can be optimized to meet the desired specifications. Our ultimate goal consists in enhancing single-mode selection for telecommunication purposes, where single-mode lasers are preferred for long-distance message transmission. In fact, in multimode lasers, modes competition might cause errors during the transmission of the information. The interplay between end-facets coatings and DFB grating structure determines the capability of selecting a single longitudinal mode of the FP cavity. In this perspective, our simulations disclosed that the combination of highly reflective coating on the back facet and anti-reflective coating on the front facet of the laser with DFB structure, whose κ_{DFB} is appropriately small, is the best option for enhancing the performances of the device in terms of single-mode selection and power efficiency. Future studies will investigate the impact of other critical dynamic phenomena, such as the effect of external optical feedback (EOF) and level of intensity and phase noise, on single-mode emission of DFB QCLs. Experimental evidences revealed a route to chaos typical for a class A laser [47] in a DFB QCL in EOF configuration, without an undamping of relaxation oscillations, contrasting with the scenarios known in interband laser diodes [48]. The onset of chaos might be utilized on niche applications of DFB QCLs, e.g. secure chaotic communications [9]. A more rigorous theoretical treatment might furnish a deeper understanding and a more realistic interpretation of the experimental outcomes. As an instance, the role of the physical and geometrical parameters in presence of optical feedback will be inspected.

References

[1] L. Sterczewski et al., "I multiheterodyne spectroscopy using interband cascade lasers," *Opt. Eng.*, vol. 57, 2018, Art. no. 011014.

[2] P. Didier et al., "Interband cascade technology for energy-efficient mid-infrared free-space communication," *Photon. Res.*, vol. 11, no. 4, pp. 582–590, Apr. 2023. [Online]. Available: https://opg.optica.org/prj/abstract.cfm?URI=prj-11-4-582

[3] N. Prasad, A. Majumdar, and J. Ricklin, *Optical Communications in the Mid-Wave IR Spectral Band*. Berlin, Germany: Springer, 2010, pp. 347–391.

[4] C. Sauvage, "Impact de l'environnement atmosphérique sur les liaisons optiques sans fil pour la ville du futur," , Ph.D. Thesis, Inst. Polytechnique de Paris, 2020.

[5] R. W. Fenn et al., "Chapter 18 optical and infrared properties of the atmosphere," 1985. [Online]. Available: https://api.semanticscholar.org/CorpusID:19595452

[6] J. J. Liu, B. L. Stann, K. K. Klett, P. S. Cho, and P. M. Pellegrino, "Mid and long-wave infrared free-space optical communication," *Proc. SPIE*, vol. 11133, 2019, Art. no. 1113302.

[7] R. McClatchey, and J. Selby,, "Atmospheric attenuation of laser radiation from 0.76 to 31.25 micrometers," ser. AFCRL-TR. air force Cambridge Research Laboratories, air force systems command, United States Air Force, 1974. [Online]. Available: https://books.google.fr/books?id=wei2zgEACAAJ

[8] P. Corrigan, R. Martini, E. A. Whittaker, and C. Bethea, "Quantum cascade lasers and the kruse model in free space optical communication," *Opt. Exp.*, vol. 17, no. 6, pp. 4355–4359, 2009.

[9] O. Spitz et al., "Private communication with quantum cascade laser photonic chaos," *Nature Commun.*, vol. 12, no. 1, 2021, Art. no. 3327.

[10] J. Faist, F. Capasso, D. L. Sivco, C. Sirtori, A. L. Hutchinson, and A. Y. Cho, "Quantum cascade laser," *Science*, vol. 264, no. 5158, pp. 553–556, 1994.

[11] B. Meng, J. Tao, X. H. Li, Y. Q. Zeng, S. Wu, and Q. J. Wang, "Tunable single-mode slot waveguide quantum cascade lasers," *Appl. Phys. Lett.*, vol. 104, no. 20, 2014, Art. no. 201106.

[12] C. Gmachl et al., "Single-mode, tunable distributed-feedback and multiple-wavelength quantum cascade lasers," *IEEE J. Quantum Electron.*, vol. 38, no. 6, pp. 569–581, Jun. 2002.

[13] L. Coldren, S. Corzine, and M. Mašanović, *Mirrors and Resonators for Diode Lasers*. Hoboken, NJ, USA: Wiley, 2012, pp. 91–155.

[14] M. Carras, M. Garcia, X. Marcadet, O. Parillaud, A. D. Rossi, and S. Bansropun, "Top grating index-coupled distributed feedback quantum cascade lasers," *Appl. Phys. Lett.*, vol. 93, no. 1, 2008, Art. no. 011109.

[15] M. Carras et al., "Room-temperature continuous-wave metal grating distributed feedback quantum cascade lasers," *Appl. Phys. Lett.*, vol. 96, no. 16, 2010, Art. no. 161105.

[16] L. L. Columbo, S. Barbieri, C. Sirtori, and M. Brambilla, "Dynamics of a broad-band quantum cascade laser: From chaos to coherent dynamics and mode-locking," *Opt. Exp.*, vol. 26, no. 3, pp. 2829–2847, 2018.

[17] A. Siegman, *Lasers, (G. - Reference, Information and Interdisciplinary Subjects Series)*. Mill Valley, CA, USA: University Science Books, 1986. [Online]. Available: https://books.google.fr/books?id=1BZVwUZLTkAC

[18] R. Lang and A. Yariv, "Intermodal stability of a coupled-cavity semiconductor laser," *IEEE J. Quantum Electron.*, vol. 22, no. 5, pp. 631–636, May 1986.

[19] H. A. Haus, "Mode-locking of lasers," *IEEE J. Sel. Topics Quantum Electron.*, vol. 6, no. 6, pp. 1173–1185, Nov./Dec. 2000.

[20] F. Capasso, C. Gmachl, D. L. Sivco, and A. Y. Cho, "Quantum cascade lasers," *Phys. Today*, vol. 55, no. 5, pp. 34–40, 2002.

[21] A. Gordon et al., "Multimode regimes in quantum cascade lasers: From coherent instabilities to spatial hole burning," *Phys. Rev. A*, vol. 77, 2008, Art. no. 053804.

[22] P. Vankwikelberge, F. Buytaert, A. Franchois, R. Baets, P. Kuindersma, and C. Fredriksz, "Analysis of the carrier-induced FM response of DFB lasers: Theoretical and experimental case studies," *IEEE J. Quantum Electron.*, vol. 25, no. 11, pp. 2239–2254, Nov. 1989.

[23] A. Takemoto et al., "Low harmonic distortion distributed feedback laser diode and module for CATV systems," in *Proc. Opt. Fiber Commun. Conf.*, 1990, paper FE2.

[24] N. Opačak et al., "Spectrally resolved linewidth enhancement factor of a semiconductor frequency comb," *Optica*, vol. 8, no. 9, pp. 1227–1230, Sep. 2021. [Online]. Available: https://opg.optica.org/optica/abstract.cfm?URI=optica-8-9-1227

[25] O. Spitz, A. Herdt, J. Duan, M. Carras, W. Elsässer, and F. Grillot, "Extensive study of the linewidth enhancement factor of a distributed feedback quantum cascade laser at ultra-low temperature", Vol. 10926, Proc. SPIE, Quantum Sensing and Nano Electronics and Photonics XVI, p. 1092619, 2019.

[26] L. Jumpertz, M. Carras, K. Schires, and F. Grillot, "Regimes of external optical feedback in 5.6μm distributed feedback mid-infrared quantum cascade lasers," *Appl. Phys. Lett.*, vol. 105, no. 13, 2014, Art. no. 131112.

[27] R. P. Green et al., "Linewidth enhancement factor of terahertz quantum cascade lasers," *Appl. Phys. Lett.*, vol. 92, no. 7, 2008, Art. no. 071106.

[28] C. Silvestri, L. L. Columbo, M. Brambilla, and M. Gioannini, "Coherent multi-mode dynamics in a quantum cascade laser: Amplitude-and frequency-modulated optical frequency combs," *Opt. Exp.*, vol. 28, no. 16, pp. 23846–23861, 2020.

[29] B. Tromborg, H. Olesen, X. Pan, and S. Saito, "Transmission line description of optical feedback and injection locking for Fabry-Perot and DFB lasers," *IEEE J. Quantum Electron.*, vol. 23, no. 11, pp. 1875–1889, Nov. 1987.

[30] C. Silvestri et al., "Theory and modelization of quantum cascade laser dynamics: Comb formation, field structures and feedback-based imaging," Ph.D. dissertation, Politecnico di Torino, Torino, Italy, 2022.

[31] C. Silvestri, X. Qi, T. Taimre, K. Bertling, and A. D. Rakić, "Frequency combs in quantum cascade lasers: An overview of modeling and experiments," *APL Photon.*, vol. 8, no. 2, 2023, Art. no. 020902, doi: 10.1063/5.0134539.

[32] M. Piccardo and F. Capasso, "Laser frequency combs with fast gain recovery: Physics and applications," *Laser Photon. Rev.*, vol. 16, no. 2, 2022, Art. no. 2100403. [Online]. Available: https://onlinelibrary.wiley.com/doi/abs/10.1002/lpor.202100403

[33] R. Paiella, *Intersubband Transitions in Quantum Structures*, (McGraw-Hill Nanoscience and Technology Series). New York, NY, USA: McGraw-Hill LLC, 2010. [Online]. Available: https://books.google.fr/books?id=cNBdGCr3Zf0C

[34] L. Jumpertz et al., "Measurements of the linewidth enhancement factor of mid-infrared quantum cascade lasers by different optical feedback techniques," *AIP Adv.*, vol. 6, 2016, Art. no. 015212.

[35] I. Vurgaftman and J. Meyer, "Analysis of limitations to wallplug efficiency and output power for quantum cascade lasers," *J. Appl. Phys.*, vol. 99, no. 12, 2006, Art. no. 123108.

[36] B. G. Lee et al., "DFB quantum cascade laser arrays," *IEEE J. Quantum Electron.*, vol. 45, no. 5, pp. 554–565, May 2009.

[37] B.-S. Kim, Y. Chung, and J.-S. Lee, "An efficient split-step time-domain dynamic modeling of DFB/DBR laser diodes," *IEEE J. quantum Electron.*, vol. 36, no. 7, pp. 787–794, Jul. 2000.

[38] H. Soda, Y. Kotaki, H. Sudo, H. Ishikawa, S. Yamakoshi, and H. Imai, "Stability in single longitudinal mode operation in GaInAsP/InP phase-adjusted DFB lasers," *IEEE J. Quantum Electron.*, vol. 23, no. 6, pp. 804–814, Jun. 1987.

[39] P. Vankwikelberge, G. Morthier, and R. Baets, "CLADISS-a longitudinal multimode model for the analysis of the static, dynamic, and stochastic behavior of diode lasers with distributed feedback," *IEEE J. Quantum Electron.*, vol. 26, no. 10, pp. 1728–1741, Oct. 1990.

[40] S. Uchiyama and K. Iga, "A 1.59 μm wavelength GainAsp/InP distributed feedback laser with first-order grating on anti-meltback layer," *Japanese J. Appl. Phys.*, vol. 22, no. 6A, 1983, Art. no. L348.

[41] C. Y. Wang et al., "Coherent instabilities in a semiconductor laser with fast gain recovery," *Phys. Rev. A*, vol. 75, no. 3, 2007, Art. no. 031802.

[42] L. Lugiato, F. Prati, and M. Brambilla, *Nonlinear Optical Systems*. Cambridge, U.K.: Cambridge Univ. Press, 2015.

[43] N. Vukovic, J. Radovanovic, V. Milanovic, and D. L. Boiko, "Analytical expression for Risken-Nummedal-Graham-Haken instability threshold in quantum cascade lasers," *Opt. Exp.*, vol. 24, no. 23, pp. 26911–26929, Nov. 2016. [Online]. Available: https://opg.optica.org/oe/abstract.cfm?URI=oe-24-23-26911

[44] T. S. Mansuripur et al., "Single-mode instability in standing-wave lasers: The quantum cascade laser as a self-pumped parametric oscillator," *Phys. Rev. A*, vol. 94, Dec. 2016, Art. no. 063807. [Online]. Available: https://link.aps.org/doi/10.1103/PhysRevA.94.063807

[45] F. Grillot, "On the effects of an antireflection coating impairment on the sensitivity to optical feedback of AR/HR semiconductor DFB lasers," *IEEE J. Quantum Electron.*, vol. 45, no. 6, pp. 720–729, Jun. 2009.

[46] G. Morthier and R. Baets, "Design of index-coupled deb lasers with reduced longitudinal spatial hole burning," *J. Lightw. Technol.*, vol. 9, no. 10, pp. 1305–1313, 1991.

[47] F. Arecchi, G. Lippi, G. Puccioni, and J. Tredicce, "Deterministic chaos in laser with injected signal," *Opt. Commun.*, vol. 51, no. 5, pp. 308–314, 1984.

[48] M. Sciamanna and K. A. Shore, "Physics and applications of laser diode chaos," *Nature Photon.*, vol. 9, no. 3, pp. 151–162, 2015.